

Group delay in THz spectroscopy with ultra-wideband log-spiral antennae

M. Langenbach,¹ A. Roggenbuck,² I. Cámara Mayorga,³ A. Deninger,²

K. Thirunavukkuarasu,^{1,4} J. Hemberger,¹ and M. Grüninger¹

¹ *II. Physikalisches Institut, Universität zu Köln, Zùlpicher Str. 77, D-50937 Köln, Germany*

² *TOPTICA Photonics AG, Lochhamer Schlag 19, D-82166 Gräfelfing, Germany*

³ *Max-Planck-Institute for Radio Astronomy, Auf dem Hùgel 69, D-53121 Bonn, Germany*

⁴ *National High Magnetic Field Laboratory, Tallahassee, Florida 32310, USA*

(Dated: June 25, 2014)

We report on the group delay observed in continuous-wave terahertz spectroscopy based on photomixing with phase-sensitive homodyne detection. We discuss the different contributions of the experimental setup to the phase difference $\Delta\varphi(\nu)$ between transmitter arm and receiver arm. A simple model based on three contributions yields a quantitative description of the overall behavior of $\Delta\varphi(\nu)$. Firstly, the optical path-length difference gives rise to a term linear in frequency ν . Secondly, the ultra-wideband log-spiral antennae effectively radiate and receive in a frequency-dependent active region, which in the most simple model is an annular area with a circumference equal to the wavelength. The corresponding term changes by roughly 6π between 100 GHz and 1 THz. The third contribution stems from the photomixer impedance. In contrast, the derivative $\partial\Delta\varphi/\partial\nu$ is dominated by the contribution of periodic modulations of $\Delta\varphi(\nu)$ caused by standing waves, e.g., in the photomixers' Si lenses. Furthermore, we discuss the Fourier-transformed spectra, which are equivalent to the waveform in a time-domain experiment. In the time domain, the group delay introduced by the log-spiral antennae gives rise to strongly chirped signals, in which low frequencies are delayed. Correcting for the contributions of antennae and photomixers yields sharp peaks or "pulses" and thus facilitates a time-domain-like analysis of our continuous-wave data.

I. INTRODUCTION

Continuous-wave (cw) terahertz spectroscopy based on photomixing is able to cover a very broad frequency range from about 0.1 THz up to 5 THz.¹ For broadband spectroscopy, it is desirable that the photomixers in combination with the antennae provide a rather smooth spectrum without pronounced resonances, i.e., a nearly frequency-independent radiation pattern and a nearly frequency-independent radiation resistance. This can be achieved by using a self-complementary antenna such as the log-spiral (or equiangular spiral) antenna,² which offers a large bandwidth in combination with a high terahertz efficiency and an excellent beam pattern.³⁻⁵ However, the log-spiral antenna effectively radiates and receives terahertz waves from the frequency-dependent annular "active region"⁶⁻⁸ with a circumference roughly equal to the wavelength λ . Therefore this antenna shows a pronounced frequency dependence of the group delay

$$t_{\text{gr}}(\nu) = \frac{1}{2\pi} \frac{\partial\varphi_{\text{an}}}{\partial\nu} \quad (1)$$

where $\varphi_{\text{an}}(\nu)$ denotes the phase of the wave emitted at frequency ν . The group delay of the antenna corresponds to the traveling time of the photocurrent from the inner feed to the active region. This delay may vary strongly over the useable frequency range of the antenna. In our case, it varies by more than a factor of 10 between 0.1 THz and 1 THz. Accordingly, log-spiral antennae are not well suited for experiments in the time domain, as a log-spiral antenna fed with a narrow pulse emits a strongly chirped signal.

In frequency-domain terahertz spectroscopy based on homodyne detection, we measure the phase difference

$\Delta\varphi(\nu)$ between transmitter arm and receiver arm, see below. The phase shift ϕ_{sam} introduced by a given sample is determined by comparison with the data measured in a reference run without sample,

$$\phi_{\text{sam}}(\nu) = \Delta\varphi_{\text{with}}(\nu) - \Delta\varphi_{\text{w/o}}(\nu). \quad (2)$$

In an ideal case, the group delay introduced by the antennae is identical in both terms on the right hand side, hence it does not contribute to $\phi_{\text{sam}}(\nu)$. Nevertheless, it is instructive to quantitatively understand the phase difference $\Delta\varphi_{\text{w/o}}(\nu)$ measured in the reference run, e.g., for a discussion of the uncertainty of the phase caused by a drift of the frequency, cf. Sec. VI. Moreover, a quantitative description of the reference phase allows for a correction of the frequency dependence of the group delay and thus facilitates a time-domain-like analysis of the cw data. To the best of our knowledge, the group delay of photomixers with log-spiral antennae working in the terahertz range has not been reported thus far. Here, we systematically discuss all contributions to the frequency dependence of the phase difference $\Delta\varphi(\nu)$. We employ a simple model and obtain a quantitative description of the overall behavior of $\Delta\varphi(\nu)$.

II. EXPERIMENTAL SETUP

A sketch of our experimental setup is given in Fig. 1, for details we refer to Refs. [9-12]. Continuous-wave terahertz radiation with frequency $\nu = |\nu_2 - \nu_1|$ is generated and coherently detected by illuminating two photomixers, transmitter and receiver, with the optical beat of two near-infrared lasers with frequencies ν_1 and ν_2 .

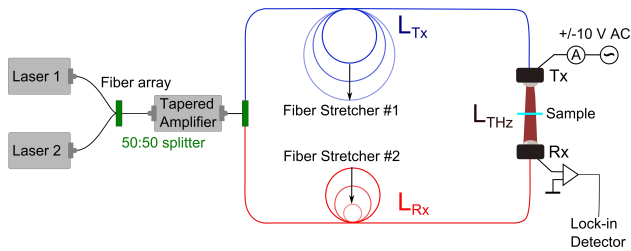


FIG. 1: Sketch of the setup. The symbols Tx and Rx refer to transmitter and receiver, respectively.

We use two laser diodes with slightly different wavelengths centered at about 780 nm, offering a maximum beat frequency of about 1.8 THz with a line width of about 5 MHz. The laser light is guided in a fiber array with two fiber-optical 50:50 splitters. The first splitter is used to superimpose the two laser beams, which are subsequently amplified in a tapered semiconductor amplifier. The second fiber-optical splitter separates the transmitter arm and the receiver arm.

In order to obtain information on both amplitude and phase, we employ fast phase modulation via two fiber stretchers¹¹ in the optical path before the photomixers, i.e., where both laser frequencies are superimposed. The two stretchers operate with opposite signs, thus changing the optical path-length difference

$$\Delta L = L_{Tx} + L_{THz} - L_{Rx} \quad (3)$$

between the transmitter arm including the THz path with the total optical path length $L_{Tx} + L_{THz}$ on the one side, and the receiver arm with the optical path length L_{Rx} on the other side.

The photomixers are based on ion-implanted GaAs and have been described in Ref. [13]. The photomixing area with dimensions of $9 \times 9 \mu\text{m}^2$ consists of an interdigitated metal-semiconductor-metal structure with eight fingers, see Fig. 2. The metallization consists of a 10/200 nm thick Ti/Au layer. The patterned antennae are self-complementary log-periodic spirals with three turns. The spiral radius $r(\alpha)$ as a function of the angle α is described by

$$r(\alpha) = r_{\min} e^{a\alpha} \quad (4)$$

with the minimum radius $r_{\min} \approx 10 \mu\text{m}$ and growth rate $a = 0.2$. With three turns, the maximum radius amounts to $r_{\max} \approx 0.43 \text{ mm}$. The outer spiral antenna arms are bonded in order to bias the photomixer structure in the case of the transmitter, or to measure the DC photocurrent of the receiver.

Due to the large dielectric constant of $\varepsilon(\text{GaAs}) = 12.8$, the antenna radiates mainly into the substrate. For an efficient coupling to free space, each photomixer is mounted on a hyper-hemispherical lens made of high-resistivity Si. Terahertz radiation is emitted with a full opening angle of only 10° at 100 GHz, 4° at 350 GHz, and $\leq 2^\circ$ between 600 GHz and 1.2 THz.¹¹ For a short distance of

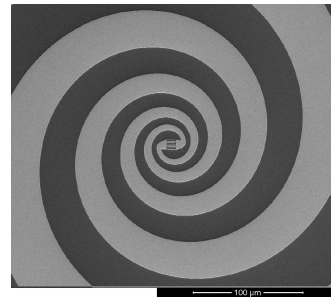


FIG. 2: Log-spiral antenna and interdigitated finger structure.

$L_{THz} \lesssim 30 \text{ cm}$ between the two photomixers, this allows us to employ a face-to-face configuration without any further focussing optics.

III. RESULTS

Based on homodyne detection, the photocurrent I_{ph} in the receiver is given by¹⁴

$$I_{\text{ph}} \propto E_{\text{THz}} \cos(\Delta\varphi), \quad (5)$$

where E_{THz} denotes the amplitude of the incident terahertz electric field and $\Delta\varphi$ the phase difference between the optical signal and the terahertz signal at the receiver. Experimentally, $\Delta\varphi$ is determined only up to an offset $m \cdot 2\pi$, where m is an integer number. However, to reveal the optical properties of a given sample we have to consider $m_{\text{with}} - m_{\text{w/o}}$, i.e., the difference between sample and reference run (cf. Eq. 2). By measuring over a broad frequency range and comparison with the model derived below, the ambiguity of m can be resolved.

Representative data of $\Delta\varphi(\nu)$ measured for different values of ΔL are depicted in Fig. 3. These data sets were obtained in reference runs without any sample. The dominant behavior at high frequencies is linear in frequency. At low frequencies, we observe strong deviations from linearity, which is most obvious for small values of ΔL .

The frequency dependence of $\Delta\varphi(\nu)$ is related to the group delay difference Δt_{gr} by

$$\Delta t_{\text{gr}} = \frac{1}{2\pi} \frac{\partial \Delta\varphi(\nu)}{\partial \nu}, \quad (6)$$

where $\Delta t_{\text{gr}}(\nu)$ describes the difference in traveling time between transmitter arm and receiver arm for a wave packet centered at ν . Let us first consider the most simple case without dispersion, i.e., a frequency-independent propagation velocity c in combination with a frequency-independent optical path-length difference ΔL_0 without any further group delays. Then, $\Delta t_{\text{gr}}(\nu) = \Delta L_0/c$ is independent of frequency, giving rise to a linear behavior $\Delta\varphi \propto \nu$. In the following, we systematically address all contributions to $\Delta\varphi(\nu)$: (1) the fibers, (2) the photomixers including the antennae and the hyper-hemispherical

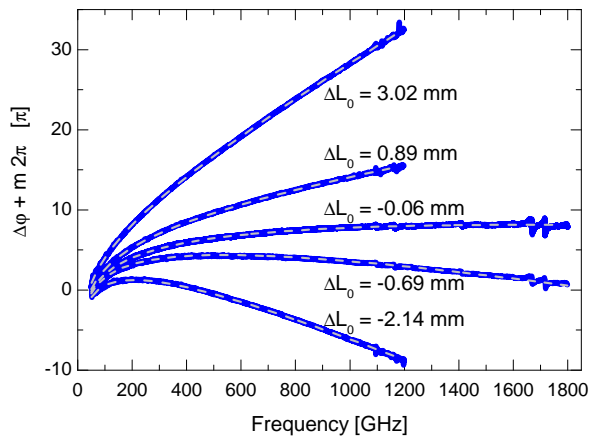


FIG. 3: Blue: Representative data sets of $\Delta\varphi(\nu)$ measured in a face-to-face configuration of the two photomixers. Different values of the optical path-length difference ΔL were obtained by changing $L_{\text{THz}} \approx 22$ cm. The frequency step width equals 100 MHz for $\Delta L \approx -0.06$ mm and 1 GHz for all other data sets. Grey: calculated values of $\Delta\varphi_{\text{mod}}(\nu)$ according to Eq. 18 with the fit parameters $\Delta\varphi_{\text{an}}(\nu_{\text{max}}) = 0.27\pi$ and ΔL_0 as given in the plot. The comparison between model and measured data yields $m \cdot 2\pi = 8\pi$.

Si lenses, and (3) the terahertz path L_{THz} including, e.g., air with water vapor or standing waves between, e.g., the photomixers.

(1) *Fibers*: The refractive index n_f of a fiber of length L_f depends on the frequencies of the two near-infrared lasers. A terahertz frequency $\nu = \nu_2 - \nu_1$ is selected by scanning the two laser frequencies symmetrically around the center frequency $\nu_0 = (\nu_1 + \nu_2)/2$, i.e., $\nu_{2,1} = \nu_0 \pm \nu/2$. The phase of the optical beat is given by

$$\varphi = L_f \cdot [n_f(\nu_2) \cdot \nu_2 - n_f(\nu_1) \cdot \nu_1] \cdot \frac{2\pi}{c}. \quad (7)$$

We assume that the dispersion is linear around 780 nm, which indeed is the case for the fiber material SiO_2 with $\partial n/\partial \nu = 4 \cdot 10^{-5}/\text{THz}$.¹⁵ We expand around the center frequency ν_0 ,

$$n_f(\nu_2) = n_f(\nu_0) + \left. \frac{\partial n_f}{\partial \nu} \right|_{\nu_0} \cdot (\nu_2 - \nu_0) = n_f(\nu_0) + \left. \frac{\partial n_f}{\partial \nu} \right|_{\nu_0} \cdot \frac{\nu}{2}, \quad (8)$$

$$n_f(\nu_1) = n_f(\nu_0) + \left. \frac{\partial n_f}{\partial \nu} \right|_{\nu_0} \cdot (\nu_1 - \nu_0) = n_f(\nu_0) - \left. \frac{\partial n_f}{\partial \nu} \right|_{\nu_0} \cdot \frac{\nu}{2}, \quad (9)$$

and find

$$\varphi = L_f \cdot \left(n_f(\nu_0) + \left. \frac{\partial n_f}{\partial \nu} \right|_{\nu_0} \cdot \nu_0 \right) \cdot \frac{2\pi\nu}{c} = L_f \cdot n_{f,\text{eff}} \cdot \frac{2\pi\nu}{c}. \quad (10)$$

The term in parentheses is independent of frequency. Due to the fact that the two lasers are scanned in opposite directions, the linear frequency dependence of n_f simply gives rise to a slight increase $n_{f,\text{eff}}/n_f \approx 1.01$ of the

frequency-independent effective fiber length $n_{f,\text{eff}} \cdot L_f$ relevant for the optical beat. The contribution of the fibers thus reads

$$\Delta\varphi_f = (L_{\text{Tx}} - L_{\text{Rx}}) \cdot \frac{2\pi\nu}{c}, \quad (11)$$

where L_{Rx} and L_{Tx} include the effective frequency-independent refractive index $n_{f,\text{eff}}$ of the fibers.

(2) *Photomixers and antennae*: We consider the following contributions: (i) coupling the optical beat into the photoactive area, (ii) the photoconductance, (iii) the photomixer impedance, (iv) the antenna, and (v) coupling to free space via a hyper-hemispherical Si lens.

(i) We utilize two identical photomixers. The effect of coupling the optical beat into the photoactive area is thus identical in the receiver arm and the transmitter arm. Hence it does not contribute to $\Delta\varphi$.

(ii) The same applies to the photoconductance G , which depends on the terahertz frequency due to the finite carrier lifetime $\tau \approx 0.5$ ps.¹³ This gives rise to a phase shift of $\varphi_G = \arctan(2\pi\nu\tau)$ in both receiver and transmitter.^{16,17} In the transmitter, the terahertz wave is delayed with respect to the optical beat, which effectively increases L_{Tx} . However, the phase shift in the receiver effectively increases L_{Rx} by the same amount. Therefore, the photoconductance does not contribute to $\Delta\varphi$.

(iii) The total impedance of photomixer and antenna effectively is described by a characteristic time constant $\tau_{RC} = R_A C$, where $R_A \approx 73\Omega$ denotes the nearly frequency-independent antenna resistivity of the log-spiral antenna on a GaAs substrate,^{5,13} and $C \approx 1.5$ fF is the capacitance of the interdigitated electrode structure.¹³ The time constant $\tau_{RC} \approx 0.1$ ps gives rise to a phase shift of $\varphi_{RC} = \arctan(2\pi\nu\tau_{RC})$, again in both receiver and transmitter. However, this phase shift has to be attributed to the transmitter arm in both photomixers. Hence both terms add up and yield a contribution of

$$\Delta\varphi_{RC} = 2 \arctan(2\pi\nu\tau_{RC}). \quad (12)$$

(iv) It is well known that ultra-wideband log-spiral antennae exhibit a strong dispersion and thus distort short pulses.^{2,7,8,18,19} The antenna effectively radiates and receives terahertz waves in an annular “active region” with radius r_{ar} , the size of which depends on frequency. Physically, the antenna predominantly radiates where the contributions from the two neighboring spiral arms interfere constructively,^{6,18} see Sec. IV. In the limit of a vanishing or very small spiral growth rate a (cf. Eq. 4), a centered log-spiral antenna radiates where the circumference equals the wavelength, $2\pi r_{\text{ar}} = \lambda$. Comparing two waves at high and low frequencies, the low-frequency wave is delayed because it has to travel a longer path $l(\nu)$ in the antenna.¹⁹ In time, the signal has to travel for

$$t_{\text{gr,an}}(\nu) = l(\nu) \cdot n_{\text{eff}}/c \quad (13)$$

where $t_{\text{gr,an}}$ is the group delay of the antenna and n_{eff} denotes the effective refractive index. With $\varepsilon(\text{GaAs}) = 12.8$,

we use $n_{\text{eff}} = \sqrt{(12.8 + 1)/2} \approx 2.6$ for the guided mode at the GaAs-air interface. The path length in the spiral equals

$$\begin{aligned} l(\alpha(\nu)) &= \int_0^\alpha \sqrt{r(\alpha')^2 + \left(\frac{dr}{d\alpha'}\right)^2} d\alpha' \\ &= \frac{\sqrt{1+a^2}}{a} (r_{\text{ar}}(\nu) - r_{\text{min}}). \end{aligned} \quad (14)$$

The inner and outer truncations of the spiral define a minimum and maximum wavelength, respectively. With the radius $r_{\text{ar}} = \lambda/2\pi$ of the active region and $r_{\text{min}} = 10 \mu\text{m}$ we find $\nu_{\text{max}} = c/(2\pi r_{\text{min}} n_{\text{eff}}) \approx 1.8 \text{ THz}$ as well as $\nu_{\text{min}} \approx 40 \text{ GHz}$ and

$$l(\nu) = \frac{c}{2\pi n_{\text{eff}}} \frac{\sqrt{1+a^2}}{a} \cdot \left(\frac{1}{\nu} - \frac{1}{\nu_{\text{max}}}\right). \quad (15)$$

With Eq. 13 we integrate Eq. 1 from ν_{max} to ν ,

$$\begin{aligned} \int_{\nu_{\text{max}}}^\nu t_{\text{gr}} d\nu &= \int_{\nu_{\text{max}}}^\nu \frac{\sqrt{1+a^2}}{2\pi a} \cdot \left(\frac{1}{\nu} - \frac{1}{\nu_{\text{max}}}\right) d\nu \\ &= \frac{1}{2\pi} [\varphi_{\text{an}}(\nu) - \varphi_{\text{an}}(\nu_{\text{max}})]. \end{aligned} \quad (16)$$

Moreover, we assume that the delay is identical upon emission and detection. In both cases, the delay effectively prolongs the transmitter arm, thus we have to add up the two contributions. This finally yields the contribution of the antenna characteristics to the phase difference $\Delta\varphi(\nu)$ between the two arms,

$$\Delta\varphi_{\text{an}}(\nu) = \frac{2\sqrt{1+a^2}}{a} \left[\ln\left(\frac{\nu}{\nu_{\text{max}}}\right) - \frac{\nu}{\nu_{\text{max}}} + 1 \right] + \Delta\varphi_{\text{an}}(\nu_{\text{max}}), \quad (17)$$

where the offset $\Delta\varphi_{\text{an}}(\nu_{\text{max}})$ is treated as a fit parameter.

(v) Standing waves within the hyper-hemispherical Si lenses give rise to a periodic modulation of $\Delta\varphi(\nu)$.^{20,21} This effect can be neglected for the discussion of the overall behavior of $\Delta\varphi(\nu)$. However, these standing waves are important if one considers the derivative $\partial\Delta\varphi/\partial\nu$, see Sec. VI.

(3) *Terahertz path:* The terahertz path length L_{THz} and the effective fiber lengths L_{Tx} and L_{Rx} constitute the optical path-length difference ΔL , contributing a term $\Delta L \cdot \frac{2\pi\nu}{c}$ to $\Delta\varphi(\nu)$, see Eqs. 3 and 11. Due to water vapor in the terahertz path and standing waves between, e.g., the photomixers, L_{THz} effectively depends on the frequency ν . For the discussion of the overall behavior of $\Delta\varphi(\nu)$, these effects are small compared to the contribution $\Delta\varphi_{\text{an}}(\nu)$ of the antenna. Therefore, we first consider a constant value of L_{THz} and come back to these smaller effects below.

Having addressed all the different contributions, we derive a simple model for the overall behavior of $\Delta\varphi(\nu)$ by taking into account the antenna contribution (cf. Eq. 17), the photomixer impedance (cf. Eq. 12), and a constant optical path-length difference ΔL_0 ,

$$\Delta\varphi_{\text{mod}}(\nu) = \Delta\varphi_{\text{an}}(\nu) + \Delta\varphi_{RC}(\nu) + \Delta L_0 \cdot \frac{2\pi\nu}{c}. \quad (18)$$

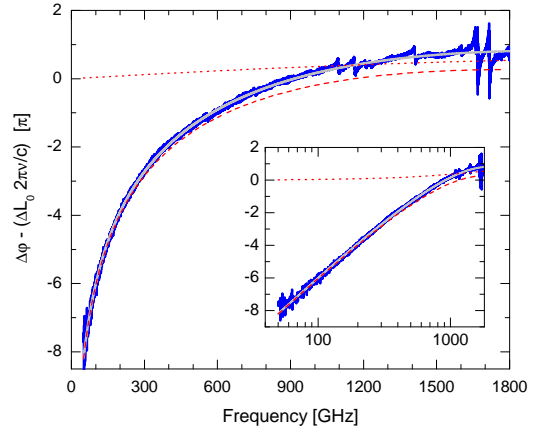


FIG. 4: Comparison of measured data and model, focussing on the non-linear contributions. Blue: $\Delta\varphi(\nu) - \Delta L_0 \cdot 2\pi\nu/c$ for the data set with $\Delta L \approx -0.06 \text{ mm}$, cf. Fig. 3. Dashed and dotted red lines depict $\Delta\varphi_{\text{an}}$ and $\Delta\varphi_{RC}$, respectively, which add up to $\Delta\varphi_{\text{mod}}(\nu) - \Delta L_0 \cdot 2\pi\nu/c$ (grey), cf. Eq. 18. Inset: same data on a logarithmic frequency scale.

For a quantitative comparison with the experimental results, we use the given values of the lifetime $\tau_{RC} = R_A C = 0.1 \text{ ps}$, the spiral growth rate $a = 0.2$, and $\nu_{\text{max}} = 1.8 \text{ THz}$. For the radius r_{ar} of the active region, we employ $2\pi r_{\text{ar}} = \lambda$ (cf. Sec. IV), leaving only two free parameters, ΔL_0 and a constant offset denoted by $\Delta\varphi_{\text{an}}(\nu_{\text{max}})$, cf. Eq. 17. Surprisingly, this simple model is in excellent agreement with our experimental data of $\Delta\varphi(\nu)$, see Fig. 3. If we view $\gamma = \lambda/2\pi r_{\text{ar}}$ as an additional fit parameter, we find $\gamma = 0.997$ and $\Delta\varphi_{\text{an}}(\nu_{\text{max}}) = 0.26\pi$.

In order to highlight the non-linear terms $\Delta\varphi_{\text{an}}(\nu)$ and $\Delta\varphi_{RC}(\nu)$, we compare $\Delta\varphi(\nu) - \Delta L_0 \cdot 2\pi\nu/c$ with $\Delta\varphi_{\text{an}}(\nu) + \Delta\varphi_{RC}(\nu)$ in Fig. 4. The antenna contribution $\Delta\varphi_{\text{an}}(\nu)$ clearly dominates since it changes by roughly 6π between 100 GHz and 1 THz.

Finally, we define an effective, frequency-dependent optical path-length difference $\Delta L_{\text{eff}}(\nu)$ and a corrected phase difference $\Delta\varphi_{\text{corr}}(\nu)$ by subtracting the two dominant non-linear terms from $\Delta\varphi(\nu)$,

$$\begin{aligned} \Delta L_{\text{eff}}(\nu) \cdot \frac{2\pi\nu}{c} &= \Delta\varphi_{\text{corr}}(\nu) \\ &= \Delta\varphi(\nu) - \Delta\varphi_{\text{an}}(\nu) - \Delta\varphi_{RC}(\nu). \end{aligned} \quad (19)$$

The result is shown in Fig. 5. The average of the effective optical path-length difference $\Delta L_{\text{eff}}(\nu)$ equals ΔL_0 , while the frequency dependence of $\Delta L_{\text{eff}}(\nu)$ and accordingly of $\Delta\varphi_{\text{corr}}(\nu)$ contains all deviations between the measured $\Delta\varphi(\nu)$ and $\Delta\varphi_{\text{mod}}(\nu)$. Due to the excellent agreement between $\Delta\varphi(\nu)$ and $\Delta\varphi_{\text{mod}}(\nu)$, the frequency dependence of $\Delta L_{\text{eff}}(\nu)$ highlights the smaller contributions that we have neglected thus far, i.e., the effective frequency dependence of L_{THz} . We identify three main contributions: (a) Standing waves within the Si lenses give rise to a modulation of ΔL_{eff} with a period of about 4.1 GHz, see inset of Fig. 5. (b) Standing waves between

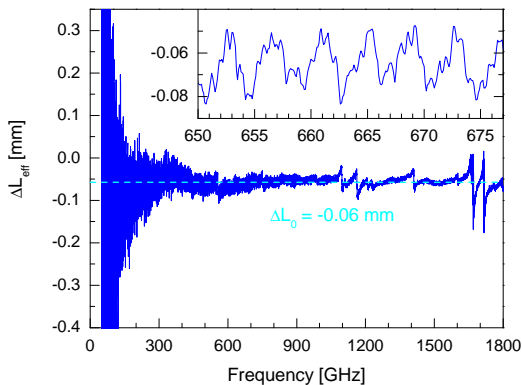


FIG. 5: Effective optical path-length difference $\Delta L_{\text{eff}}(\nu)$ for the data set with $\Delta L \approx -0.06$ mm, cf. Eq. 20 and Fig. 3. Inset: same data on a larger scale, showing the 4.07 GHz modulation stemming from the Si lenses of the photomixers as well as the 0.7 GHz modulation caused by standing waves between the photomixers for $L_{\text{THz}} \approx 22$ cm.

the two photomixers separated by $L_{\text{THz}} \approx 22$ cm cause a modulation period of $0.7 \text{ GHz} \approx c/0.4 \text{ m}$. These periodic features are well resolved in the Fourier-transformed data, see Sec. V. (c) We observe resonant absorption features of water vapor.^{23,24} The absorption lines are very well resolved even for this comparably short path in air. Very roughly, the absorption line at 557 GHz is expected to cause a peak-to-peak change of about $2 \cdot 10^{-4}$ of the refractive index of air.²⁴ For $L_{\text{THz}} \approx 22$ cm, this corresponds to about $40 \mu\text{m}$ peak-to-peak, in rough agreement with our data.

IV. ACTIVE REGION

The antenna radiates most strongly from a region in which the two spiral arms radiate in phase, giving rise to constructive interference.^{6,18} For the radius r_{ar} of the active region, we consider a spot with $r_{\text{ar}} = (r_+ + r_-)/2$ which is located between the two neighboring arms with radii r_- and $r_+ = r_- \cdot e^{a\pi}$, respectively. There, the path length of the two neighboring arms differs by $l(r_+) - l(r_-) = l(\alpha + \pi) - l(\alpha)$, cf. Eq. 14. The antenna is fed in a balanced way, thus the currents in the two arms are out-of-phase at $\pm r_{\text{min}}$. Constructive interference occurs if the path-length difference between the two arms equals $\lambda/2$, compensating for the initial phase shift of π . With Eqs. 4 and 14 we find

$$\frac{\lambda}{2} = l(\alpha + \pi) - l(\alpha) = \frac{\sqrt{1 + a^2}}{a} (r_- - r_{\text{min}}) \cdot (e^{a\pi} - 1). \quad (20)$$

Neglecting $r_{\text{min}} \approx 10 \mu\text{m} \ll \lambda$, the radius of the active region amounts to

$$r_{\text{ar}} = \frac{r_+ + r_-}{2} = \frac{a}{4\sqrt{1 + a^2}} \frac{e^{a\pi} + 1}{e^{a\pi} - 1} \cdot \lambda. \quad (21)$$

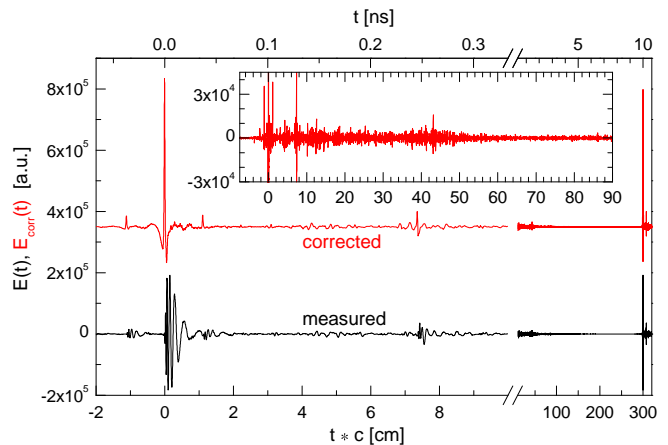


FIG. 6: Fourier series $E(t)$ of the data (black) measured up to 1.8 THz for $\Delta L \approx -0.06$ mm (cf. Fig. 3) and after correction (red), cf. Eq. 23. Data are offset for clarity. A frequency step width of 100 MHz yields $E(t)$ with a period $T \approx 300 \text{ cm}/c$. Note the change of scale at 10 cm. Inset: Corrected data on a different scale. The feature which is shifted by 7.36 cm with respect to the main peak results from standing waves in the Si lenses, the peak at 43.1 cm corresponds to $2 \cdot L_{\text{THz}}$ and is caused by standing waves between the two photomixers.

For a vanishing growth rate $a \rightarrow 0$, this yields $2\pi r_{\text{ar}} = \lambda$. For $a = 0.2$, we find $2\pi r_{\text{ar}} \approx 1.01\lambda$, in excellent agreement with our experimental result.

A theoretical study of the radiated power density as a function of $2\pi r/\lambda$ has been reported in Ref. [22] for planar log-spiral antennae with different growth rates. For $a \approx 0.18 \approx 1/\tan(80^\circ)$, the power density shows a rather broad, asymmetric peak at about $2\pi r = \lambda/2$ and decreases only slowly towards higher values of r . Integrating the contributions from $2\pi r = 0.2\lambda$ to 2λ yields a first moment of about 0.9λ , in fair agreement with our results.

V. QUASI-TIME-DOMAIN ANALYSIS

Knowing amplitude $E_{\text{THz}}(\nu)$ and phase difference $\Delta\varphi(\nu)$ for the discrete set of frequency points of a certain measurement, one can easily calculate the Fourier series as a function of the time t ,

$$E(t) = \sum_{\nu} E_{\text{THz}}(\nu) \cos(2\pi\nu t - \Delta\varphi(\nu)), \quad (22)$$

an approach which has been called quasi-time-domain analysis.²⁵ The Fourier series is equivalent to an interferogram or to the waveform in a time-domain terahertz experiment, where all frequencies are measured simultaneously.

In the Fourier series, the main peak is expected at $t = \Delta L/c$. The measured data of $E(t)$ (black line in Fig. 6) do not show well-defined peak positions, but are strongly asymmetric around any peak. This is the typical shape of a down-chirp signal, in which the higher

frequencies arrive first, reflecting the strongly frequency-dependent group delay introduced by the antenna. However, using the corrected phase difference $\Delta\varphi_{\text{corr}}(\nu)$ (cf. Eq. 20) in the Fourier series

$$E_{\text{corr}}(t) = \sum_{\nu} E_{\text{THz}}(\nu) \cos(2\pi\nu t - \Delta\varphi_{\text{corr}}(\nu)) \quad (23)$$

removes the strong down-chirp and yields a pronounced “pulse” at the expected position (red line in Fig. 6). The remaining peak width reflects the finite bandwidth of the experiment and in particular the strong decrease of the amplitude with increasing frequency. The corrected data also show a clear feature shifted by 7.36 cm with respect to the main peak, which is equivalent to a period of 4.07 GHz. This feature reflects the periodic modulations shown in the inset of Fig. 5, i.e., standing waves in the Si lenses. Peaks at $t \cdot c = \pm 1.1$ cm are due to standing waves in the tapered amplifier. These occur before the optical path is split into two arms and thus do not contribute to $\Delta\varphi$, i.e., they are only observed in the amplitude. The feature at 43.1 cm reflects standing waves between the two photomixers with $L_{\text{THz}} \approx 22$ cm. We also observe an overtone at about 86 cm. Using the corrected data clearly facilitates the detection and precise determination of such features in the Fourier series.

VI. GROUP DELAY AND UNCERTAINTY OF THE PHASE

The uncertainty $\delta\varphi$ of the measured phase difference $\Delta\varphi(\nu)$ depends on the experimental uncertainties of ΔL and ν ,

$$\delta\varphi = \frac{\partial\Delta\varphi}{\partial\nu} \cdot \delta\nu + \frac{2\pi\nu}{c} \cdot \delta L. \quad (24)$$

In our setup, the optical path-length difference is typically stable to within $\delta L = \pm 5 \mu\text{m}$.¹¹ The line width of the beat signal of the two widely tunable lasers amounts to about 5 MHz, while a long-term frequency stability of better than 20 MHz over 24 h was observed.⁹ On the time scale of less than 1 h, the frequency stability is better than $\delta\nu = 5$ MHz. The quantitative understanding of $\Delta\varphi(\nu)$ achieved in the previous sections allows us to discuss the importance of the different contributions to the group delay difference $\Delta t_{\text{gr}} \propto \partial\Delta\varphi/\partial\nu$, i.e., to the first term on the right hand side. We consider (cf. Eq. 20)

$$\frac{\partial\Delta\varphi}{\partial\nu} = \frac{\partial\Delta\varphi_{\text{an}}}{\partial\nu} + \frac{\partial\Delta\varphi_{\text{RC}}}{\partial\nu} + \Delta L_{\text{eff}} \cdot \frac{2\pi}{c} + \frac{\partial\Delta L_{\text{eff}}}{\partial\nu} \cdot \frac{2\pi\nu}{c}. \quad (25)$$

For the first two terms we find

$$\begin{aligned} \frac{\partial\Delta\varphi_{\text{an}}}{\partial\nu} &= \frac{2\sqrt{1+a^2}}{a} \cdot \left(\frac{1}{\nu} - \frac{1}{\nu_{\text{max}}} \right) \\ \frac{\partial\Delta\varphi_{\text{RC}}}{\partial\nu} &= \frac{4\pi\tau_{\text{RC}}}{1 + (2\pi\nu\tau_{\text{RC}})^2}. \end{aligned} \quad (26)$$

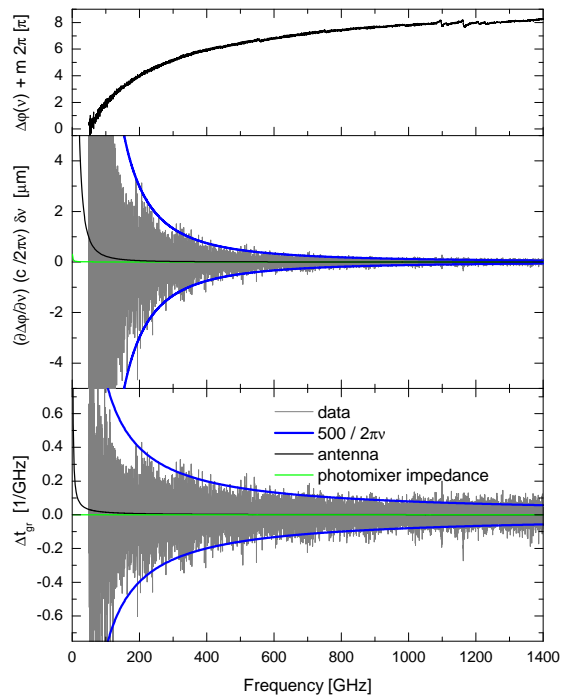


FIG. 7: Top: phase difference $\Delta\varphi(\nu)$ for $\Delta L \approx -0.06$ mm, cf. Fig. 3, measured with a frequency step width of 100 MHz. Bottom: group delay difference $\Delta t_{\text{gr}} = (\partial\Delta\varphi/\partial\nu)/2\pi$ compared to the contributions of the antennae, $(\partial\Delta\varphi_{\text{an}}/\partial\nu)/2\pi$ (black), and of the photomixer impedance, $(\partial\Delta\varphi_{\text{RC}}/\partial\nu)/2\pi$ (green). Blue: rough estimate of the envelope. Middle: Same data as in the bottom panel, multiplied by $(c/\nu)\delta\nu$ with $\delta\nu = 5$ MHz, for comparison with a length change δL , cf. Eq. 27.

The term $\Delta L_{\text{eff}} \cdot 2\pi/c$ dominates for large values of ΔL but can be suppressed by choosing a small ΔL . For instance, it amounts to about 0.2/GHz for $\Delta L = 1$ cm. The data shown in Fig. 7 was measured with $\Delta L \approx -0.006$ cm (cf. Fig. 5), thus the third term in Eq. 25 can be neglected. The comparison with experimental data in Fig. 7 shows that the first two terms can equally be neglected. Although the contributions of $\Delta\varphi_{\text{an}}$ and $\Delta\varphi_{\text{RC}}$ dominate the overall behavior of $\Delta\varphi(\nu)$, they are both negligible with respect to the derivative $\partial\Delta\varphi/\partial\nu$. This derivative is dominated by the remaining term $\propto \partial\Delta L_{\text{eff}}/\partial\nu$, i.e., by the contribution of standing waves within the Si lenses and between the two photomixers. Empirically, we find that the envelope of $\partial\Delta\varphi/\partial\nu$ is roughly described by $f(\nu) = \pm 500/\nu$ for $\Delta L \approx -0.06$ mm and $L_{\text{THz}} \approx 22$ cm, see bottom panel of Fig. 7.

In order to compare the effects of frequency uncertainty versus length drift, we consider

$$\delta\varphi \cdot \frac{c}{2\pi\nu} = \frac{\partial\Delta\varphi}{\partial\nu} \cdot \frac{c}{2\pi\nu} \cdot \delta\nu + \delta L. \quad (27)$$

With $\delta\nu = 5$ MHz and the experimental result for the envelope of $\pm 500/\nu$, the first term roughly yields $0.12 \mu\text{m} \cdot (\text{THz}/\nu)^2$, which amounts to $3 \mu\text{m}$ at 200 GHz or $0.75 \mu\text{m}$ at 400 GHz, see middle panel of Fig. 7. The typical length

drift observed in our setup equals $\pm 5 \mu\text{m}$.¹¹ We conclude that for $\delta L = \pm 5 \mu\text{m}$, $\Delta L \lesssim 1 \text{ cm}$, and frequencies above about 200 GHz, the uncertainty $\delta\varphi/\nu$ mainly depends on the drift of the optical path-length difference, in agreement with the experimental results discussed in Ref. [11].

VII. CONCLUSIONS

We investigated the phase difference $\Delta\varphi(\nu)$ between transmitter arm and receiver arm in cw terahertz spectroscopy based on photomixers with ultra-wideband log-spiral antennae. We find that $\Delta\varphi(\nu)$ and the group delay difference $\Delta t_{\text{gr}} \propto \partial\Delta\varphi/\partial\nu$ are dominated by different terms. The overall behavior of $\Delta\varphi(\nu)$ is quantitatively described by taking into account three different contributions. The optical path-length difference gives rise to a term linear in frequency, while the radiation charac-

teristics of the log-spiral antennae and the photomixer impedance cause deviations from this linear behavior. The contribution $\Delta\varphi_{\text{an}}(\nu)$ of the log-spiral antennae is very well described by a simple model which assumes that the antennae effectively radiate and receive in an active region in which the circumference equals λ . Correcting for the group delay of the antennae and photomixers strongly facilitates an analysis of the Fourier-transformed spectra. In contrast to $\Delta\varphi(\nu)$, the derivative $\partial\Delta\varphi/\partial\nu$ is dominated by the contribution of standing waves, i.e., periodic modulations of $\Delta\varphi(\nu)$. In combination with a finite frequency error, these standing waves may affect the experimental uncertainty $\delta\varphi$, but typically their contribution can be neglected in comparison to the effect of a drift of the optical path-length difference. Nevertheless it is advisable to suppress standing waves with a small modulation period, in particular for measurements at low frequencies.

-
- ¹ K.A. McIntosh, E.R. Brown, K.B. Nichols, O.B. McMahon, W.F. DiNatale, and T.M. Lyszczarz, *Appl. Phys. Lett.* **67**, 3844 (1995).
- ² W. Wiesbeck, G. Adamiuk, and C. Sturm, *Proceedings of the IEEE* **97**, 372 (2009).
- ³ E.R. Brown, K.A. McIntosh, K.B. Nichols, and C.L. Dennis, *Appl. Phys. Lett.* **66**, 285 (1995).
- ⁴ K.A. McIntosh, E.R. Brown, K.B. Nichols, O.B. McMahon, W.F. DiNatale, and T.M. Lyszczarz, *Appl. Phys. Lett.* **69**, 3632 (1996).
- ⁵ T.K. Nguyen, T.A. Ho, H. Han, and I. Park, *J. Infrared Milli. THz Waves* **33**, 1123 (2012).
- ⁶ J.A. Kaiser, *IRE Trans. Antennas Propag.* **8**, 312 (1960).
- ⁷ M. McFadden and W.R. Scott, Jr., *IEEE Trans. Antennas Propag.* **55**, 3163 (2007).
- ⁸ M. McFadden and W.R. Scott Jr., *Microwave Opt. Techn. Lett.* **51**, 536 (2009).
- ⁹ A.J. Deninger, T. Göbel, D. Schönherr, T. Kinder, A. Roggenbuck, M. Köberle, F. Lison, T. Müller-Wirts, and P. Meissner, *Rev. Sci. Instr.* **79**, 044702 (2008).
- ¹⁰ A. Roggenbuck, H. Schmitz, A. Deninger, I. Cámara Mayorga, J. Hemberger, R. Güsten, and M. Grüninger, *New J. Phys.* **12**, 043017 (2010).
- ¹¹ A. Roggenbuck, K. Thirunavukkuarasu, H. Schmitz, J. Marx, A. Deninger, I. Cámara Mayorga, R. Güsten, J. Hemberger, and M. Grüninger, *J. Opt. Soc. Am. B* **29**, 614 (2012).
- ¹² A. Roggenbuck, M. Langenbach, K. Thirunavukkuarasu, H. Schmitz, A. Deninger, I. Cámara Mayorga, R. Güsten, J. Hemberger, and M. Grüninger, *J. Opt. Soc. Am. B* **30**, 1397 (2013).
- ¹³ I. Cámara Mayorga, E.A. Michael, A. Schmitz, P. van der Wal, R. Güsten, K. Maier, and A. Dewald, *Appl. Phys. Lett.* **91**, 031107 (2007).
- ¹⁴ S. Verghese, K.A. McIntosh, S. Calawa, W.F. Dinatale, E.K. Duerr, and K.A. Molvar, *Appl. Phys. Lett.* **73**, 3824-3826 (1998).
- ¹⁵ I.H. Malitson, *J. Opt. Soc. Amer.* **55** 1205 (1965).
- ¹⁶ I.S. Gregory, C. Baker, W.R. Tribe, I.V. Bradley, M.J. Evans, E.H. Linfield, A.G. Davies, and M. Missous, *IEEE J. Quant. Electronics* **41**, 717 (2005).
- ¹⁷ M. Tani, O. Morikawa, S. Matsuura, and M. Hangyo, *Semicond. Sci. Technol.* **20**, S151 (2005).
- ¹⁸ M. McFadden, PhD thesis, *Analysis of the equiangular spiral antenna*, Georgia Institute of Technology (2009).
- ¹⁹ T.W. Hertel and G.S. Smith, *IEEE Trans. Ant. Prop.* **51**, 1426 (2003).
- ²⁰ A.V. Boriskin, A.I. Nosich, S.V. Boriskina, T.M. Benson, P. Sewell, and A. Altintas, *Microwave Opt. Techn. Lett.* **43**, 515 (2004).
- ²¹ T. Göbel, PhD thesis, *Systeme, Verfahren und Komponenten zur hochauflösenden Dauerstrich-Terahertz-Spektroskopie*, TU Darmstadt (2010).
- ²² P. Piksa and M. Mazanek, *IEEE 6th European Conference on Antennas and Propagation (EUCAP)*, 1960 (2012). DOI: 10.1109/EuCAP.2012.6206301
- ²³ H.M. Pickett, R.L. Poynter, E.A. Cohen, M.L. Delitsky, J.C. Pearson, and H.S.P. Müller, *J. Quant. Spectrosc. Radiat. Transfer* **60**, 883 (1998).
- ²⁴ D.R. Grischkowsky, Y. Yang, and M. Mandehgar, *Opt. Express* **21**, 18899 (2013).
- ²⁵ M. Scheller and M. Koch, *Opt. Express* **17**, 17723 (2009).